AD-A067 913 ANALYTICAL METHODS INC BELLEVUE WASH F/G 20/4
A VISCOUS/POTENTIAL FLOW INTERACTION ANALYSIS FOR CIRCULATION-C--ETC(U)
MAY 78 F A DVORAK N00600-76-C-1494
UNCLASSIFIED 7710 NL

1 OF 1
ADA
067913

END
DATE
FILMED
6-79
DDC

(11) MAY 1978

(12) 52 p.

(14) ANALYTICAL METHODS REPORT NO. 7710

CONTRACT FINAL REPORT.

(9)

(6) A VISCOUS/POTENTIAL FLOW INTERACTION ANALYSIS FOR CIRCULATION-CONTROLLED AIRFOILS.

BY:

(10) F.A. DVORAK

PREPARED UNDER CONTRACT (15) N00600-76-C-1494

BY:

ANALYTICAL METHODS, INC.
100 - 116TH AVENUE S. E.
BELLEVUE, WASHINGTON 98004
(206) 454-6119

SPONSORED BY:

AVIATION AND SURFACE EFFECTS DEPARTMENT
DAVID W. TAYLOR NAVAL SHIP RESEARCH
AND DEVELOPMENT CENTER
BETHESDA, MARYLAND 20084

SUMMARY

A method developed for the analysis of the incompressible viscous flow over circulation-controlled airfoils is described. A surface vorticity method is used to solve the inviscid portion of the flow and a combination of integral and finite difference methods is used to calculate the development of the viscous layers. An iterative process is used to arrive at final solutions which satisfy an appropriate trailing-edge condition and incorporate the interaction between the viscous and potential regions of the flow. Comparisons between calculated and experimental results show good agreement for surface pressure distributions and lift coefficients over a range of blowing momentum coefficient from 0 to 0.12. A discussion of the possibility of Coanda jet detachment when circulation-controlled airfoils are operating at high subsonic Mach Numbers is included in an Appendix.

PREFACE

This program was sponsored by The Naval Air Systems Command and the David W. Taylor Naval Ship Research and Development Center of the U.S. Navy. The technical work was monitored by Mr. R.M. Williams of the Aviation and Surface Effects Department of the David W. Taylor Naval Ship Research and Development Center. The program was authorized by Contract N00600-76-C-1494.

The author wishes to thank Mr. R.M. Williams, Ms. Jane Abramson and Mr. J. Wilkerson of the Aviation and Surface Effects Department for their many helpful discussions. The author also gratefully acknowledges the contribution made by Dr. R.J. Kind of Carleton University, Ottawa, while a visiting consultant on the contract during the summer of 1976.

TABLE OF CONTENTS

LIST OF FIGURES

LIST OF FIGURES CONTINUED

Nomenclature

c	airfoil chord length
C_L	lift coefficient, based on airfoil chord length
C_p	static pressure coefficient
C_μ	blowing momentum coefficient, $J/\frac{1}{2}\rho U_\infty^2 c$
H	boundary layer shape factor, δ^*/θ
J	blowing momentum flux per unit span
J_{ex}	excess momentum flux in wall jet, per unit span
K	pressure gradient parameter, $(\theta^2/\nu)(dU/ds)$
ℓ	length of panels used to represent airfoil
N	number of panels used to represent airfoil
p	static pressure
q	surface source strength (volume efflux per unit surface area)
R	radius of curvature
R_θ	momentum thickness Reynolds number, $U\theta/\nu$
s	arc length along airfoil surface
u,v	flow velocity components in potential flow analysis
U	local flow velocity at outer edge of viscous layer
U_∞	free stream velocity
γ	strength per unit area of surface vorticity distribution
Γ	circulation around airfoil
δ	boundary layer displacement thickness
θ	boundary layer momentum-defect thickness
ν	fluid viscosity
ρ	fluid density

Subscripts

ins	denotes laminar boundary layer instability
sepl	denotes separation of lower surface flow
sepu	denotes separation of upper surface flow
slot	denotes conditions at blowing slot
trans	denotes transition

INTRODUCTION

This report represents the results of the second phase of the development of an analysis method for circulation-control airfoils. During the first phase, which was reported in March, 1975 (Ref. 1), the basic analysis procedure was assembled and attempts were made to analyse circulation-controlled airfoils. A major difficulty with the "Kutta" condition soon became apparent. Because the trailing-edge is round rather than sharp, the position of the rear stagnation point is not known a priori. Consequently a trial and error approach was used; that is, a guess was made as to the location of the rear stagnation point, and the trailing-edge region was panelled in such a way that the Kutta condition could be applied at that point. Although the approach showed promise, it was soon apparent that a geometry lofting procedure would be required to re-panel the trailing-edge region at each iteration between the potential flow and viscous flow calculations. This would be required in order that the rear stagnation point, the location of which is directly related to the locations of the upper and lower surface separation points, could be fixed at each iteration. At the beginning of the current phase of work, it soon became apparent that if a relofting procedure were adopted, it would necessitate re-inversion of the aerodynamic influence coefficient matrix at each iteration between potential and viscous flows. This would result in a considerable increase in computer time, and would negate the advantages gained in using the source method (instead of adding displacement thickness directly) to account for viscous effects. Consequently, the lofting approach has been dropped, and an alternative procedure chosen. It is this new method which is described in the following sections.

DESCRIPTION OF THE ANALYSIS METHOD

General Description

The present method is in many respects similar to methods for the analysis of the viscous flow over conventional airfoil sections; that is, sections having a sharp trailing-edge. In fact, the present computer program can treat such airfoils (with or without slot blowing) as a special case. The flow chart in Figure 1 shows the sequence of the principal steps in the analysis. The first step is a calculation of the potential flow around the airfoil. Next, boundary layer and wall jet developments are computed using pressure distributions obtained from the potential flow analysis. Then the viscous interaction effects are modeled and the potential flow analysis is repeated, and so on, until a converged solution is arrived at.

For circulation-controlled airfoils, the potential flow analysis cannot make use of conventional forms of the Kutta condition because there is no sharp trailing-edge of known position to delineate between upper surface and lower surface flows; in effect, one does not know, a priori, where the Kutta condition should be applied. To circumvent this difficulty, the Kutta condition is replaced by an equation which specifies the value of the total circulation around the airfoil; this value corresponds to an estimated value for the lift coefficient. The potential flow solution gives, among other things, the positions of the forward and aft stagnation points, and these serve as the divisions between the upper-surface flow and the lower-surface flow.

Starting at the forward stagnation point, the development of the boundary layer along the lower surface of the airfoil is calculated, and the pressure at which it separates, P_{sepl}, is determined. Starting again at the forward stagnation point, the development of the boundary layer along the upper

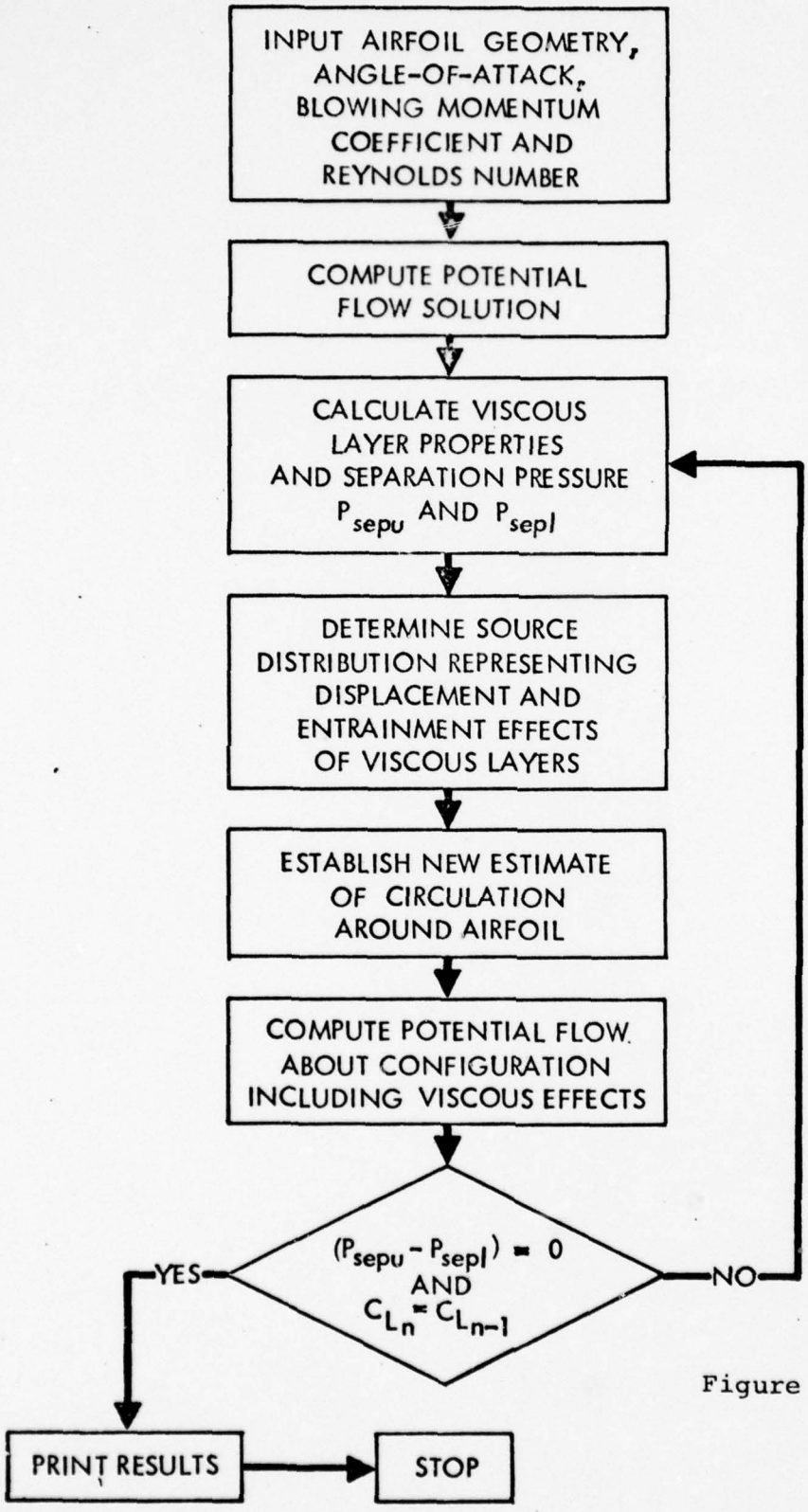

Figure 1. Calculation Procedure.

surface is calculated up to the position of the blowing slot. At the slot, another flow development calculation is initiated using an initial velocity profile made up of the boundary layer velocity profile and the assumed velocity distribution (essentially) uniform) of the blowing air at the slot exit. This development calculation proceeds until flow separation is predicted and the separation pressure, P_{sepu}, is noted. All of the aforementioned flow-development calculations use static pressure distributions given by the previous potential flow analysis.

Measured static pressure distributions around circulation-controlled airfoils clearly show that the separation pressures of the upper and lower surface flows, P_{sepu}, and P_{sepl}, are equal. This observation is physically reasonable because it merely implies that the static pressure is constant throughout the separation bubble shown in Figure 2. Experiment (Ref. 2) also indicates that there is a negligible static pressure difference across the wall jet at its separation position; the equality of P_{sepu} and P_{sepl} then implies equality of velocity in the inviscid flow leaving the upper and lower surfaces. This in turn implies that no net vorticity is being convected into the wake, which is consistent with existence of a fixed value of circulation and lift on the airfoil (Ref. 3). There is thus ample justification for assuming that the analysis has arrived at the correct solution for any particular set of conditions if P_{sepu} and P_{sepl} are equal for that solution. The goal of the iteration process is thus to find that solution which gives P_{sepu} equal to P_{sepl}.

Of course, the values of P_{sepu} and P_{sepl} calculated during the first pass through the analysis will normally not be equal to one another, and even if they were, it would be necessary to repeat the analysis in order to incorporate the viscous/

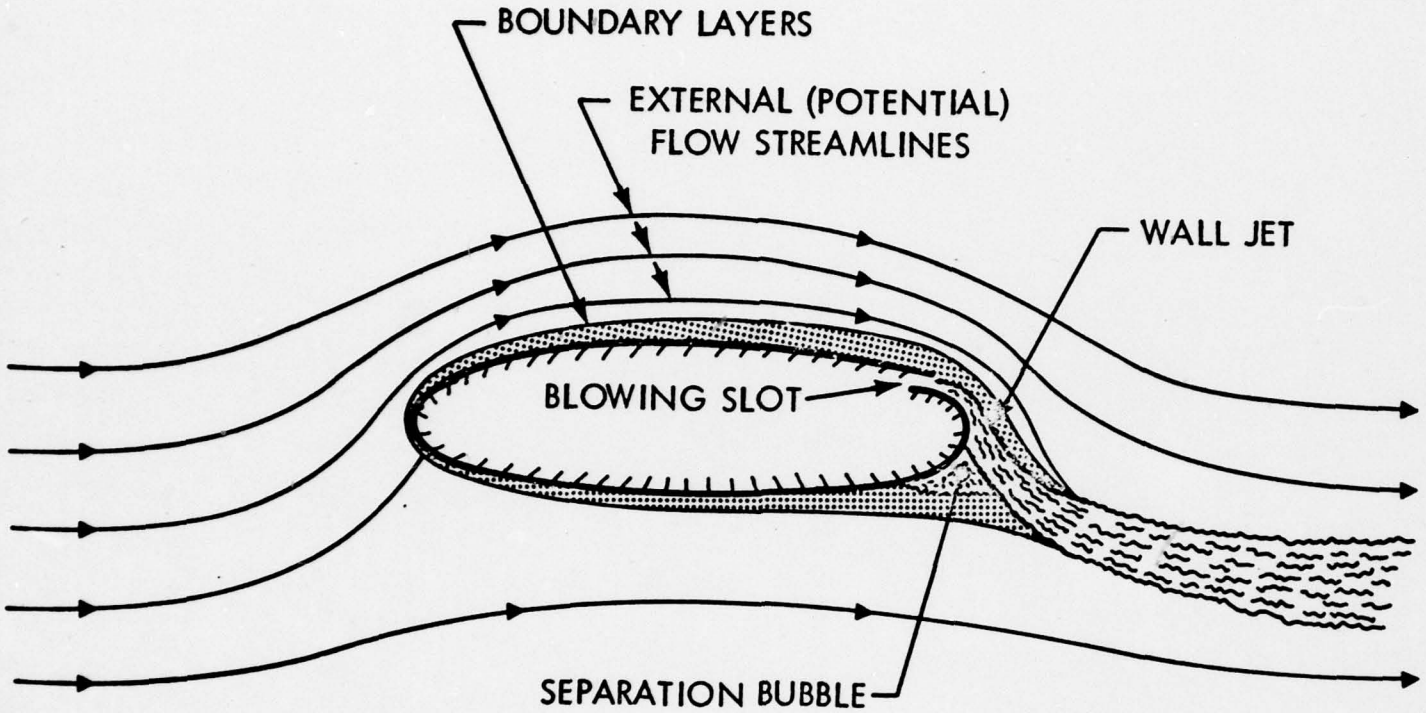

Figure 2. The Flow Over a Circulation-Controlled Airfoil.

potential flow interaction effects. To proceed then, a new value of the lift or circulation around the airfoil is estimated on the basis of the current values of lift and $(P_{sepu} - P_{sepl})$. A surface source distribution is generated to model the displacement and entrainment effects due to the viscous layers. The source distribution is incorporated into the potential flow analysis, which is then repeated with the circulation specified at the new value. The viscous flow development calculations are then repeated using the pressure distributions from the potential flow analysis, and so on. The solution is deemed to have converged to the correct result when the lift coefficient remains essentially unchanged between iterations, and at the same time $(P_{sepu} - P_{sepl})$ is essentially zero.

Description of the Major Elements of the Method

The following paragraphs describe in outline form, the major elements in the analysis method. Full details of the individual analysis procedures can be found in Reference 1.

Potential Flow Analysis

The airfoil geometry data is supplied to the program in the form of coordinates of a large number (about 60) of points on the surface. These points serve as junction points between planar panels used to represent the airfoil in the analysis. A junction point must be located at the blowing slot position. Figure 3 illustrates the paneling scheme and the notation used to describe it in this report.

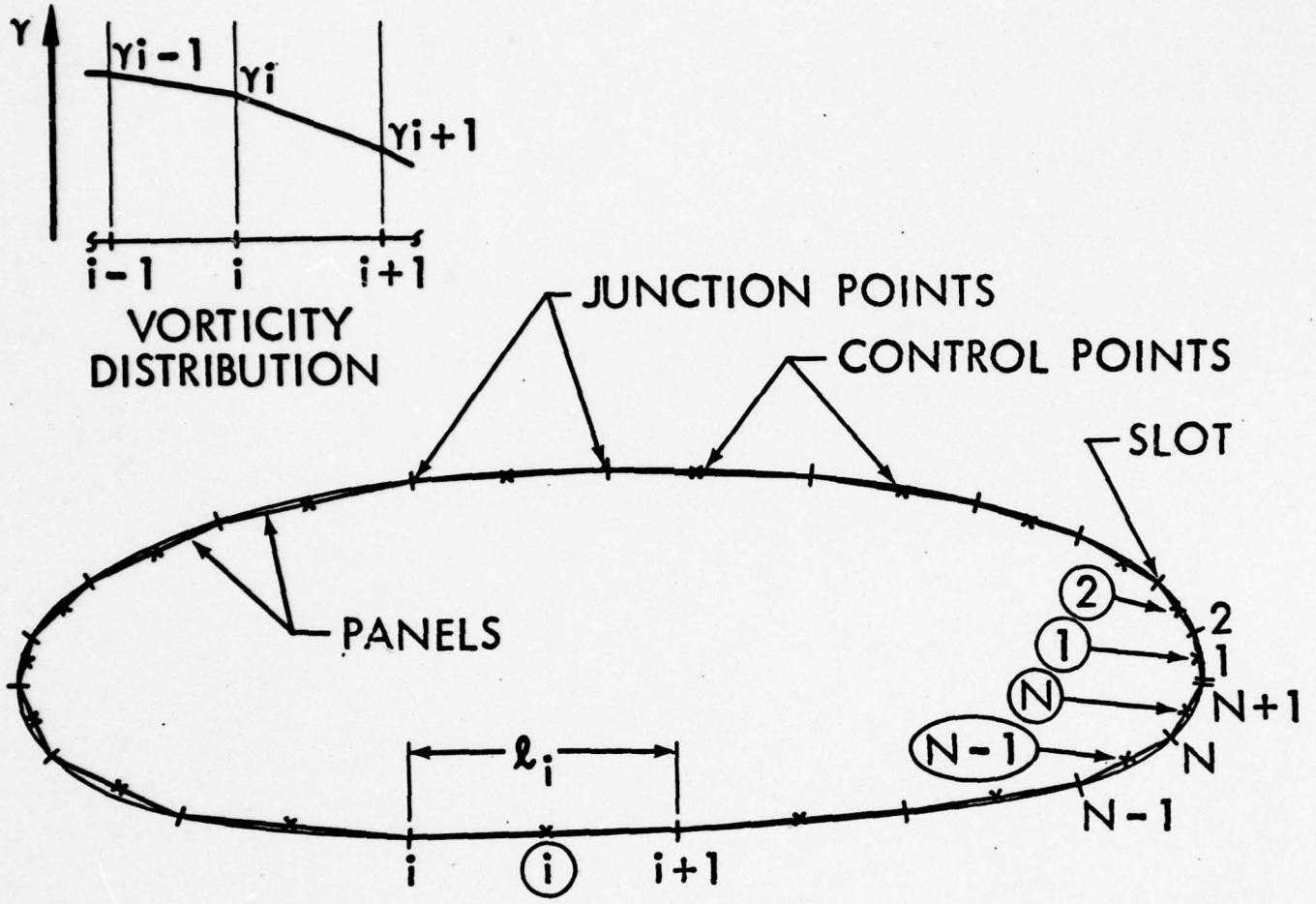

Figure 3. Airfoil Panelling Scheme.

The potential flow over the airfoil is modeled by distributing vorticity along the panels. The strength, γ, of the vortex panels or sheets is made to vary linearly along each panel, and is continuous at all junction points. Thus, if there are N panels on the airfoil, there are N unknown strengths, γ_1 to γ_N, since the vorticity values, γ_1 and γ_{n+1} will be equal. The boundary condition of zero net velocity normal to the panel surface is applied at a total of N control points, one at the midpoint of every panel. This gives a set of N equations in N unknowns. In addition, however, it is necessary to introduce an equation to specify the value of the total circulation, Γ, around the airfoil, as mentioned earlier. This equation takes the form

$$\sum_{i=1}^{N} \left[\ell_i \frac{(\gamma_i + \gamma_{i+1})}{2} \right] = \Gamma \qquad (1)$$

where ℓ_i is the length of the i^{th} panel. To avoid having a greater number of equations than unknowns, an additional unknown is provided by adding the influence of a uniform strength source distributed around the inside of the airfoil surface. It should be noted that the solution obtained for this unknown source strength is always very close to zero.

The equations are set up in matrix form with γ_1 to γ_N and the uniform source strength as unknowns. The influence coefficients of the unknowns are computed on the first pass through the analysis method and their matrix is inverted. On subsequent passes through the analysis, a surface source distribution is introduced to model viscous/potential flow interaction effects. The strength variation of this source distribution is, however, determined by the results of the viscous flow analysis so that it only introduces an additional known induced velocity on the right-hand side of each boundary condition. The total circulation Γ also appears only on the right-hand side. Therefore, the

matrix of influence coefficients is not altered, and only matrix multiplication is required to obtain the potential flow solution for the second and later iterations. A later subsection gives details of the method used to model viscous/potential flow interaction effects.

Pressure coefficients on the surface are calculated using

$$C_p = 1 - u^2 - v^2, \tag{2}$$

where u and v are the non-dimensional velocity components parallel and normal to the surface at the control points. Pressure coefficients are also calculated for a grid of off-body points in the trailing-edge region downstream of the blowing slot. The static pressure in this region varies rapidly along both tangents and normals to the airfoil surface and the information is required for the finite-difference flow development calculation used downstream of the slot. To speed convergence of the iteration process, it has been found advantageous to use a weighted average of the newly computed and previous values of the pressure coefficients in the continuing calculations.

Before proceeding to the viscous flow calculations, the potential flow solution is sought for the forward and aft stagnation points. These are considered to be located where the vorticity γ changes sign. The static pressure data generated by the potential flow analysis is then rearranged into two arrays. Each of these begins at the junction point nearest to the forward stagnation point and runs downstream, one along the upper surface and the other along the lower surface of the airfoil. Each array is terminated two junction points past the position of the rear stagnation point. These arrays are used for the viscous flow calculations which must, of course, begin essentially at the forward stagnation point for both the upper- and lower-surface flows.

The potential flow analysis method has been extensively tested in this and other applications, and it generally gives very good agreement with exact solutions. A detailed description of the basic method is available in References 1 and 4.

Boundary Layer Development Calculation Along Lower Surface

The boundary layer development calculation begins essentially at the forward stagnation point with the Heimenz stagnation flow solution (Ref. 5). As mentioned above, an array giving the static pressure distribution along the surface is provided by the potential flow analysis. Curle's (Ref. 6) extension of Thwaites' method is used for calculation of the laminar boundary layer development downstream of the stagnation point. The calculation proceeds until either transition or laminar separation is indicated.

Empirical correlations are of necessity used to predict transition. The procedure of Granville (Ref. 7) is used for this purpose. The laminar boundary layer flow becomes unstable to small disturbances when the Reynolds number based on the local momentum thickness, θ, and the local flow properties attains some critical value, $R_{\theta_{ins}}$. Schlichting and Ulrich (Ref. 8) have shown that $R_{\theta_{ins}}$ can be correlated with the local pressure gradient parameter, $(\theta^2/\nu)(dU/ds)$. Analytical expressions are used to represent the correlations. Once R_θ exceeds the critical value, $R_{\theta_{ins}}$, the transition process is assumed to begin, and Granville has been able to show that a correlation similar to that for the instability process can be used to determine the additional distance to the transition position.

With transition predicted, the turbulent boundary layer calculation is begun. The value at transition is used as the initial turbulent momentum thickness. The initial turbulent value of H is determined from the following empirical relation developed from data obtained by Coles (Ref. 9):

$$H = \frac{1.4754}{\log_{10} R_{\theta_{trans}}} + 0.9698. \qquad (3)$$

In some cases, the pressure gradient is sufficiently adverse to cause separation of the laminar boundary layer prior to transition. The flow will then usually quickly become turbulent and reattach as a turbulent boundary layer. From the measurements of Gaster (Ref. 10) and others, a correlation is formed which can predict the occurrence of both separation with subsequent reattachment and separation without reattachment. This correlation is shown in Figure 4. If separation with turbulent reattachment is predicted, the initial turbulent values of θ and H are chosen as for ordinary transition.

The turbulent boundary layer development is calculated using the Nash-Hicks method (Ref. 11). This integral method has been found to be as good as the best finite-difference methods in predicting the development of conventional boundary layers in a wide variety of pressure distributions (Ref. 12) The turbulent boundary layer calculation is continued until separation occurs, at which time its position and pressure, P_{sep1}, are noted.

Viscous Flow Development Calculation Along Upper Surface

This calculation begins at the forward stagnation point and proceeds along the upper surface to the blowing slot position using the same subroutines as the lower surface boundary layer

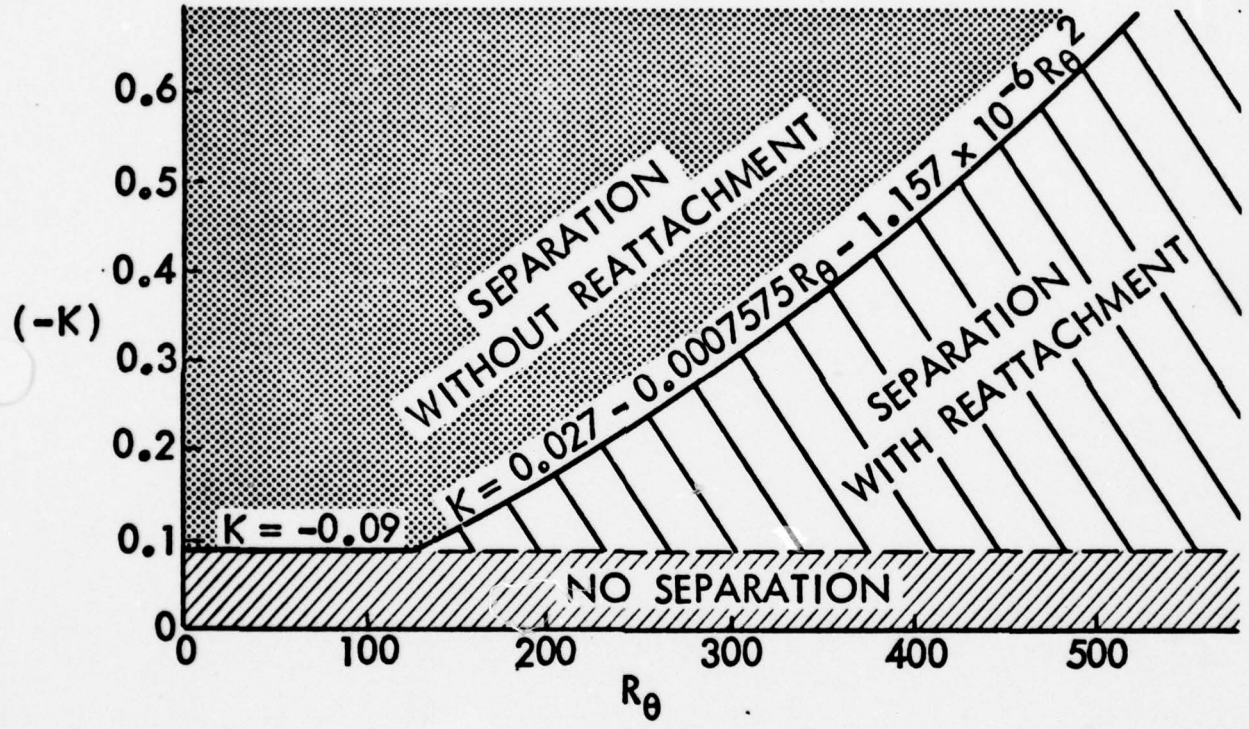

Figure 4. Laminar Separation--Turbulent Reattachment Criteria.

calculations. Normally, separation without reattachment does not occur upstream of the blowing slot, but if it does, the calculated separation position and pressure, P_{sepu}, are stored and the iteration process is continued in the usual way. Normally, the flow at the slot is attached, and it is necessary to calculate the development of the rather complex viscous flow downstream of the slot. Here, the air from the previously developed boundary layer begins mixing with the high velocity jet issuing from the slot. The flow proceeds around a highly curved surface in very strong pressure gradients, and eventually separates at some pressure, P_{sepu}.

Accurate predictions of the static pressure rise sustainable by the upper surface flow are crucial to the overall accuracy of the analysis method. The physical function of the blowing air on a circulation-controlled airfoil is to enable the upper surface flow to negotiate the static pressure rise between the aft suction peak and the final separation pressure.

The separation pressure varies weakly with the circulation due primarily to the manner in which the lower surface pressure varies. Increasing circulation typically results in a gradually decreasing adverse pressure gradient on the lower surface which allows the boundary layer to remain attached to a higher pressure level. However, the suction peak rises as the circulation around the airfoil increases. Thus stronger blowing is required to sustain the increased static pressure rise associated with increased circulation, and the circulation is directly and strongly dependent on the pressure rise that can be sustained.

As illustrated in Figure 5, a wide variety of velocity profile shapes can occur between the slot and separation; the profile shape also tends to change quite rapidly. Integral methods are not well suited to dealing with such complex and

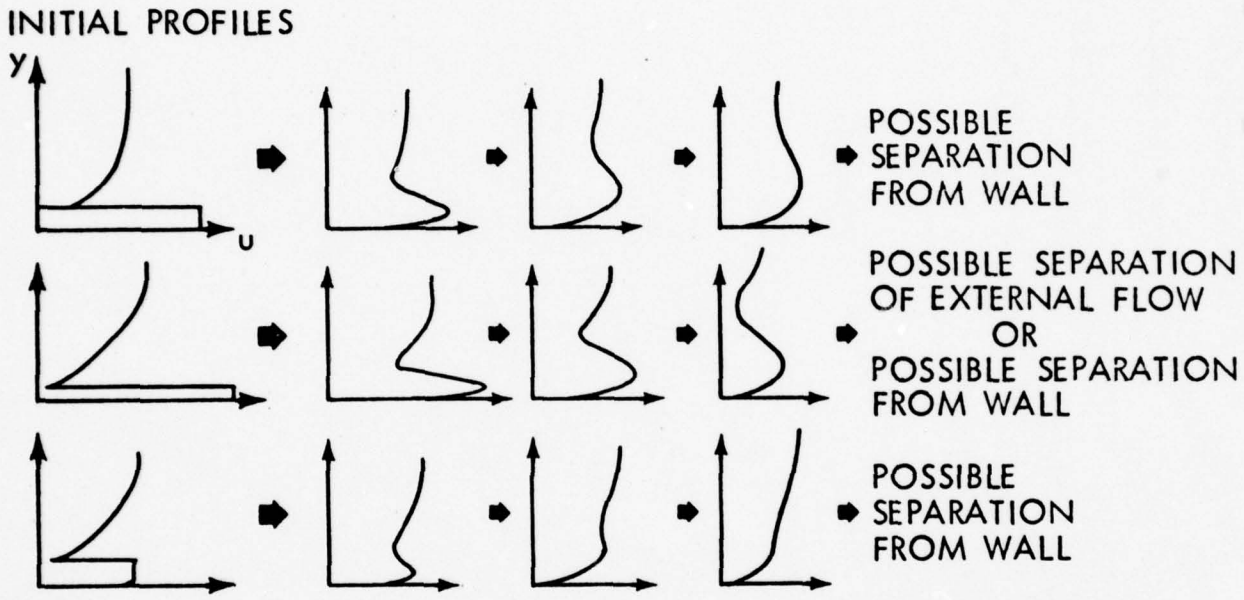

Figure 5. Possible Wall Jet Velocity Profile Shapes.

varied velocity profile shapes. The present analysis method accordingly utilizes a finite-difference method to calculate development of the viscous flow downstream of the slot. Of course, the closure assumptions used to model the Reynolds shear stress behavior are crucially important to the success of the method. The closure model must give reasonably realistic results for the types of flow being calculated, and at the same time must not be so demanding of computer time that the overall analysis method is rendered impractical. An eddy viscosity model is used in the finite-difference method employed in the present work. This method is described in References 1 and 13; it was developed for two-dimensional turbulent boundary layers and wall jets over curved surfaces, and is well suited to the present application.

The finite-difference calculation is started at the slot with an initial velocity profile consisting of the final profile from the Nash-Hicks boundary layer calculation under which is placed a nearly uniform velocity profile to represent the blowing air issuing from the slot. The shape of the initial profile is illustrated in Figure 5. The slot air is assumed to have the same density as the ambient air, and its velocity is determined such that it has the correct momentum flux assuming isentropic expansion to local static pressure determined by potential flow at the slot exit.

The surface of a circulation-control airfoil generally has a strong convex curvature downstream of the blowing slot; it is therefore necessary to account for curvature effects in the finite-difference calculations. The equations of motion are formulated with the required curvature terms, and are solved for static pressure fields which include the radial variation of static pressure due to flow curvature. The potential flow analysis gives the radial variation of static pressure where the

flow stagnation pressure is approximately equal to the free-stream value. When the free-stream value is exceeded, an additional variation is superimposed; this is assumed to vary linearly from $-(J_{ex}/R)$ at the solid surface to zero at the minimum in the velocity profile. This superimposed variation represents the extra radial pressure difference required to balance the excess momentum flux, J_{ex}, in the wall-jet portion of the flow; the assumption of linearity is approximately justified on the basis of Reference 14. The convex curvature also has a pronounced effect on the turbulence structure because the flow is radially unstable where its velocity decreases with increasing radial distance from the surface.

In the original program, the Reynolds stress term was represented by the eddy viscosity using the expression

$$\tau/\rho = -\overline{u'v'} = \nu_t(\partial u/\partial y - uk/(1 + ky)) \qquad (4)$$

where

ν_t = eddy viscosity, and

$uk/(1 + ky)$ = effect of curvature on shear stress.

This expression was first generated by Prandtl (Ref. 15), and later by Sawyer (Ref. 16). Sawyer suggested that Eqn. (4) should be written as

$$-\overline{u'v'} = \nu_t\,(\partial u/\partial y - C_1 uk/(1 + ky)) \qquad (5)$$

where for curved wall jets C_1 can take a value in the range $5 \leq C_1 \leq 9$. In the original program, a brief investigation of the impact of C_1 on the downstream velocity profile development had indicated little or no change for values of $C_1 \leq 9$; consequently, $C_1 = 1.0$ had been used. However, a more recent investigation by Wilson and Goldstein (Ref. 17) suggests that C_1 can take on much higher values, such as $C_1 = 25$ when the radius of curvature is small.

The discussion to this point has centered around the value of C_1 in the outer region of the wall jet, that is, beyond the position of U_{max}. In the region near the wall, where the shear stress must take on a positive value, it is difficult to estimate from experiment just what value of C_1 is appropriate. The experimental data of Wilson and Goldstein does, however, indicate that the region of positive shear stress is very much smaller for a curved wall jet than for a planar one. Because the velocity gradient, $\partial u/\partial y$, in Eqn. (5) is positive and large close to the wall, the implication is that C_1 must also be large in order that the shear stress will become negative a small distance away from the wall. In the region near the laminar sublayer where the velocity and shear stress fields must again be directly related, C_1 must reduce to a value approaching one.

The foregoing discussion argues for a value for C_1 which is a function of the distance from the wall. Typically, the minimum in shear stress occurs at a value of y slightly greater than that for the position of U_{max}. Consequently, a cubic expression for C_1 of the form

$$C_l = 182.\eta - 339.\eta^2 + 190.\eta^3 \qquad (6)$$

where

$$\eta = y/y_m$$

was used for the region $y \leq y_m$, while a linear expression was used for C_l in the outer region.

$$C_l = 33. - 32.\eta \qquad (7)$$

where

$$\eta = (y - y_m)/(y_{max} - y_m).$$

Unfortunately, no measured shear stress profiles on a complete circulation-controlled airfoil are available for direct comparison with calculated profiles. Calculated profiles are, however, qualitatively and quantatively similar to those measured by Jones (Ref. 18) on a quasi-circulation-controlled airfoil. The calculated velocity and shear stress profiles for a 29% ellipse having a circular arc trailing-edge are shown in Figure 6. The constants used in Eqns. (6) and (7) resulted from a numerical experiment to determine which approximate values gave the best comparison with the experimental results of Kind (pressure distributions, velocity profiles and lift coefficients). There is a great need for velocity and turbulent shear stress profile measurements on a representative circulation-controlled airfoil so that more detailed comparisons with experiment can be made for the individual calculation methods which, together, make up program CIRCON. At the moment, evaluation of the method is based on comparison of global properties of the circulation-controlled airfoils; that is, pressure distributions, lift, drag and moment coefficients.

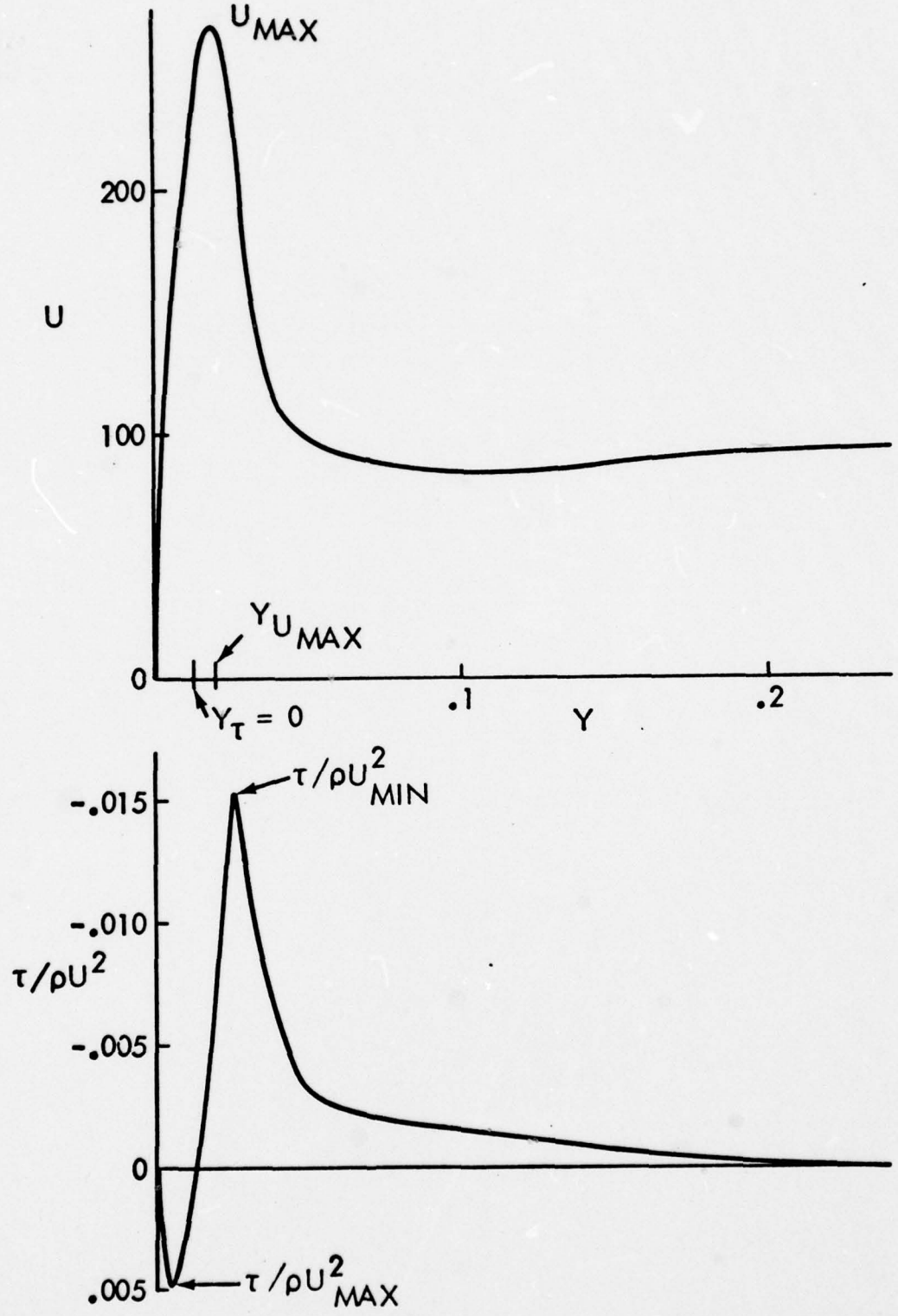

Figure 6. Typical Calculated Velocity and Shear Stress Distributions with Blowing.

Modeling Viscous/Potential Flow Interaction

Effects

As previously mentioned, surface source distributions are used to model viscous/potential flow interaction effects. This approach has two major advantages over the addition of a displacement thickness to the original airfoil geometry. First, as pointed out earlier, the matrix of aerodynamic influence coefficient remains the same for all iterations with attendant savings in computer time. Second, as pointed out in Reference 19, the addition of displacement thicknesses tends to produce peculiar surface geometries, especially in the trailing-edge region, with attendant difficulties in obtaining correct values for lift and pressure distribution; such difficulties are completely avoided when surface source distributions are used.

The source distribution is placed on the planar panels which are used to represent the airfoil. The source strength, q, varies linearly between junction points and is continuous at the junction points. At any junction point, it is given the value

$$q_i = \frac{d}{ds} (U\delta^*) \tag{8}$$

where s denotes arc length, U is the local external (inviscid) flow velocity, and δ^* is the local boundary layer displacement thickness, determined by the viscous flow analysis.

In the next pass through the potential flow analysis, the source distribution specified by Eqn. (8) produces a velocity normal to the original airfoil surface equal to that which would be produced by the addition of a displacement thickness distribution to the original airfoil contour. The effect on the inviscid flow beyond the edge of the boundary layers is thus identical. In the potential flow analysis, the boundary condition

equations ensure that the net normal velocity induced by the free stream, and by the vorticity, the uniform internal source and the specified surface source distribution is zero just inside the panel surface at every control point. With the exception of the local surface source strength at any given point, all contributions to the normal velocity are the same both just inside and just outside the panel. The only net normal velocity just outside the panel at any control point is therefore an outward velocity equal to the local surface source strength.

No special methods are needed to deal with the entrainment effects due to the wall jet downstream of the blowing slot; the product, $U\delta^*$ tends to decrease here and the source strengths then simply become negative (i.e., sinks).

The Iteration Scheme

The main features of the iteration scheme have already been outlined in a previous section. Briefly, the scheme involves estimation of lift or circulation around the airfoil, solution of the potential flow for this circulation, calculation of the viscous layer development and of the upper- and lower-surface flow separation pressures, P_{sepu} and P_{sepl}. If P_{sepu} and P_{sepl} are equal, the analysis is considered to have converged to the correct result; if not, a new estimate of circulation is generated, the surface source distribution is updated and the whole analysis is repeated.

The analysis begins with a rough estimate of the circulation. The second and subsequent estimates of circulation are obtained using

$$\Gamma_{n+1} = \Gamma_n + k \left(C_{P_{sepu}} - C_{P_{sepl}} \right) \tag{9}$$

where the numerical constant, k, has a value in the range $0.1 \leq k \leq 0.3$. This relation follows from two assumptions:

(i) At fixed angle-of-attack, an increase in circulation or in C_L corresponds to an approximately uniform increase in suction on the upper surface and little pressure change on the lower surface.

(ii) For any particular value of C_μ, an approximately fixed pressure rise, $\left(C_{P_{slot}} - C_{P_{sepu}}\right)$, can be sustained by the flow downstream of the blowing slot.

If the estimated circulation is too low relative to the correct value, a problem tends to arise. That is, the static pressure rise seen by the flow development calculation downstream of the slot is too low, and separation fron the surface is not necessarily predicted. The calculation then tends to predict reverse flow away from the wall in the boundary between the wall jet and the remnant of the upstream boundary layer. In such cases, the iteration process is continued using an estimate for the separation position and pressure based on an extrapolation to zero skin friction coefficient from the point of mid-stream reversal. The value of $C_{P_{sepu}}$ given by the extrapolation will generally be greater than $C_{P_{sepl}}$, and it is only used for obtaining the next estimate for the circulation Γ. Such external flow separation is a real but uncommon possibility on circulation-controlled airfoils. When it occurs in the calculations, it is usually only because the current estimate of circulation around the airfoil is too low.

The calculations are not allowed to stop unless at least two iterations have been completed. This ensures that the viscous/potential flow interaction effects are accounted for in the final results. The calculations are terminated when the lift coefficient remains essentially unchanged between iterations and at the same time $\left(C_{P_{sepu}} - C_{P_{sepl}}\right)$ is essentially zero.

Aerodynamic Forces

The lift and pitching moment coefficient calculations remain the same as those described in Reference 1; that is, they are determined directly from the calculated pressure distribution. The drag calculation has been considerably modified in the present program. Instead of using the Squire and Young formula (Ref. 20), which is unable to directly account for base pressure drag due to separation, the drag is determined through direct integration of the skin friction and pressure distributions around the contour of the airfoil, corrected for the thrust due to the jet, by subtracting the blowing coefficient, C_μ, from the results. Experience with conventional sharp trailing-edge airfoils suggests that drag determined from pressure integration will be consistently higher than experiment, particularly for airfoils at low angles-of-attack. The procedure will, however, be capable of predicting incremental changes in drag due to changes in configuration.

DISCUSSION OF RESULTS

The calculation method has been applied to the analysis of circulation-controlled airfoils of interest to the U.S. Navy. The case of zero momentum coefficient is of special interest in the event of blowing power loss. An example of this is shown in Figure 7, where measured and calculated pressure distribution are compared for a 29% ellipse (Ref. 21) having a circular trailing-edge. The agreement for the zero blowing case is excellent and demonstrates a capability not heretofore published in the literature.

Further calculations were made for the 29% ellipse over a range of momentum coefficients. Calculated and measured pressure distributions for a momentum coefficient of 0.088 are compared in Figure 8. The calculated and measured lift coefficient characteristics of this airfoil for a range of momentum coefficients at an angle-of-attack of -5 degrees are given on Figure 9. In general, the results for this airfoil are very encouraging.

Additional computations were made for comparison with experimental data obtained on a cambered 20% ellipse (Ref. 22), and these are shown on Figures 10 through 12. The calculated and experimental pressure distributions for momentum coefficients of 0.02 and 0.0811 are in good agreement. The lift-momentum coefficient characteristics of the cambered ellipse for an angle-of-attack range from 0 to -10 degrees are quite well reproduced as indicated on Figure 12.

Two airfoils having the same basic cambered 15% elliptical forebody, but with different trailing-edge shapes have been analysed. The airfoil designated Model 100 (NCCR 1510 - 7067N) has a circular trailing-edge, while Model 100A (NCCR 1510 - 7567S) has an inverse logarithmic spiral trailing-edge. The results shown on Figure 13 indicate excellent agreement with experiment for the circular trailing-edge model. The agreement for the

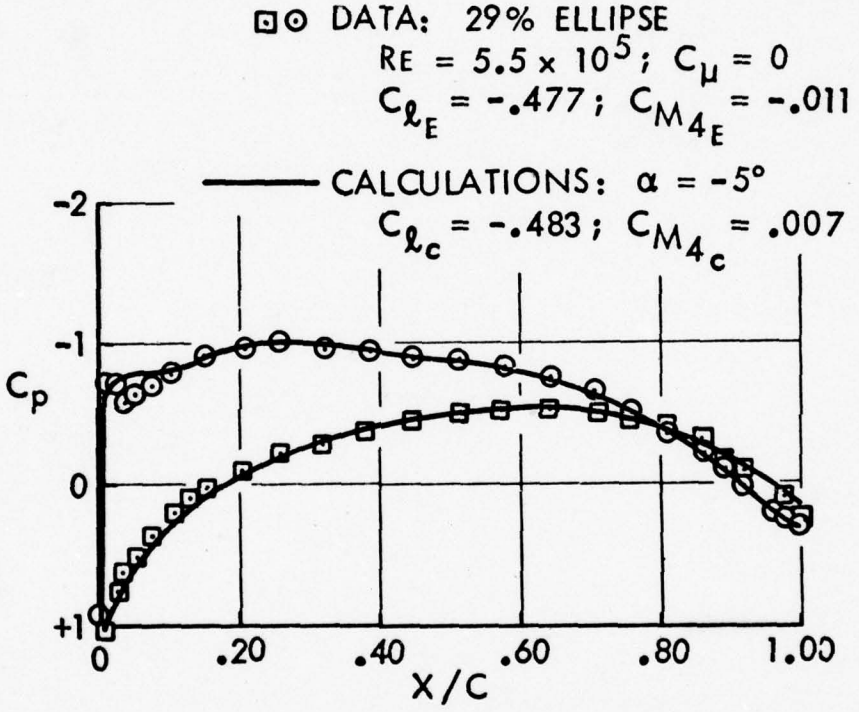

Figure 7. Comparison Between Calculated and Measured Pressure Distributions for a 29% Ellipse, $C_\mu = 0$.

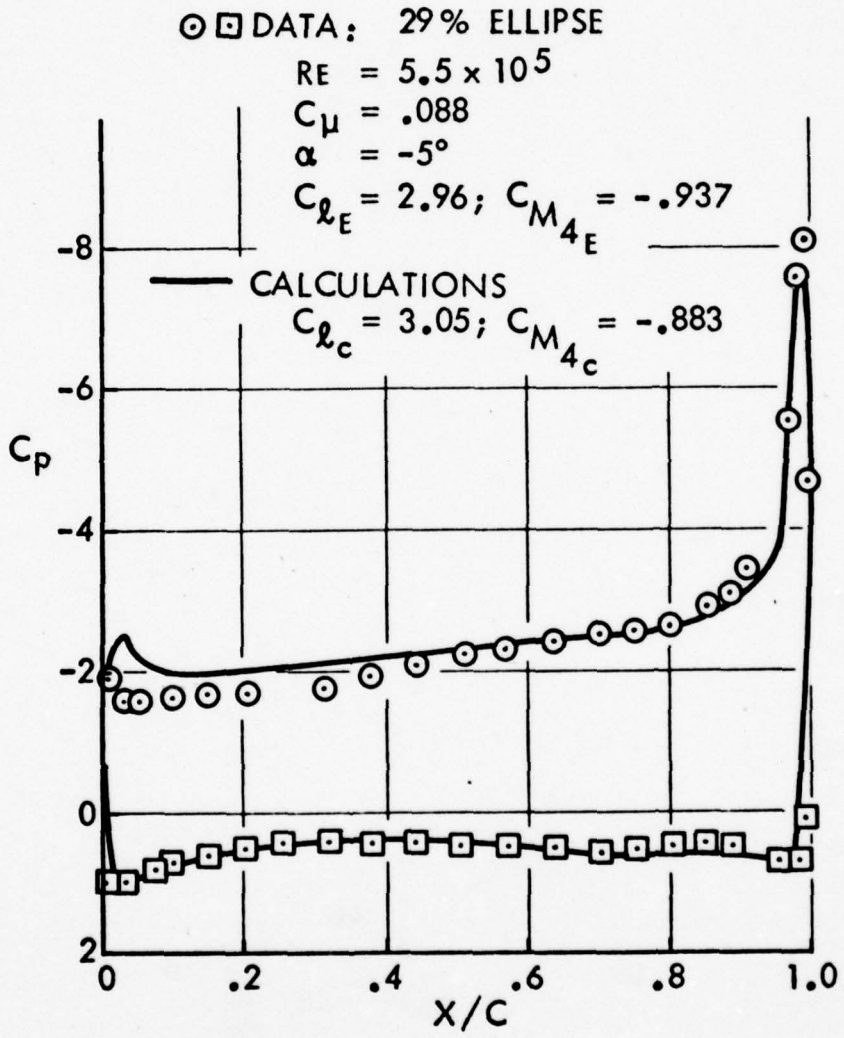

Figure 8. Comparison Between Calculated and Measured Pressure Distributions for a 29% Ellipse, C_μ = .088.

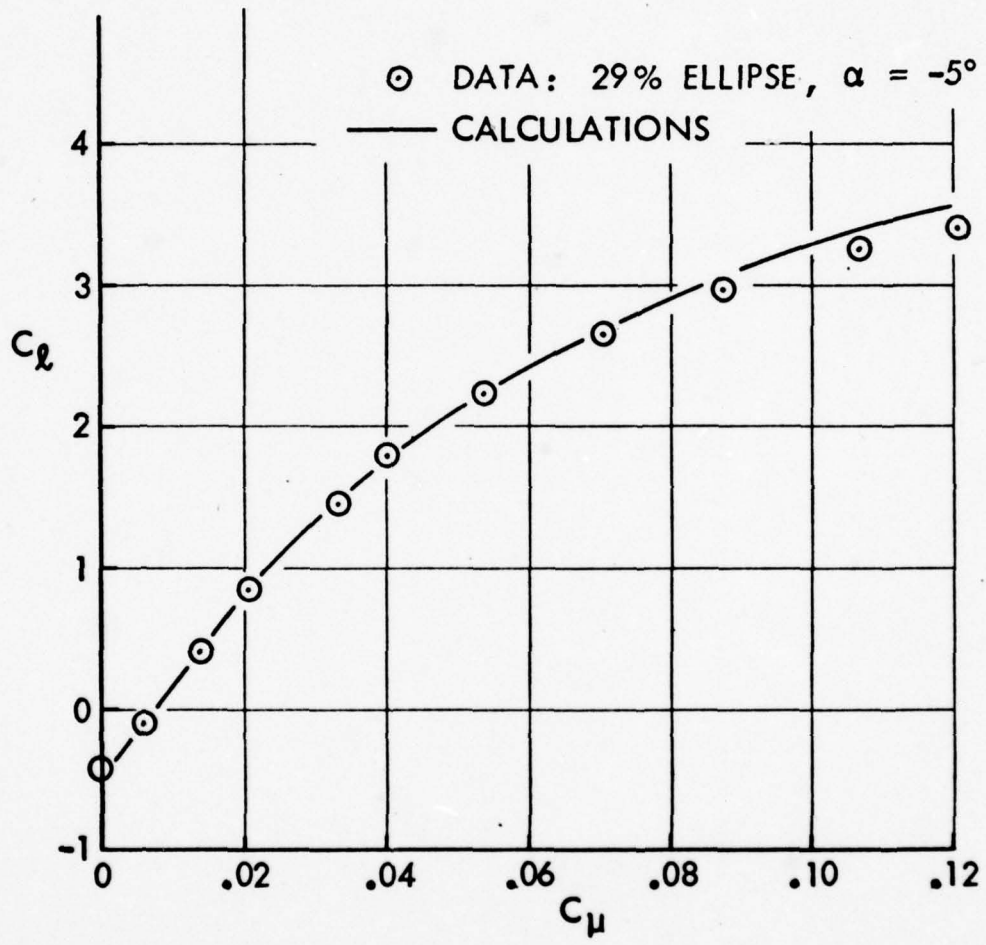

Figure 9. Comparison Between Calculated and Measured Lift Coefficients for a Range of Momentum Coefficients.

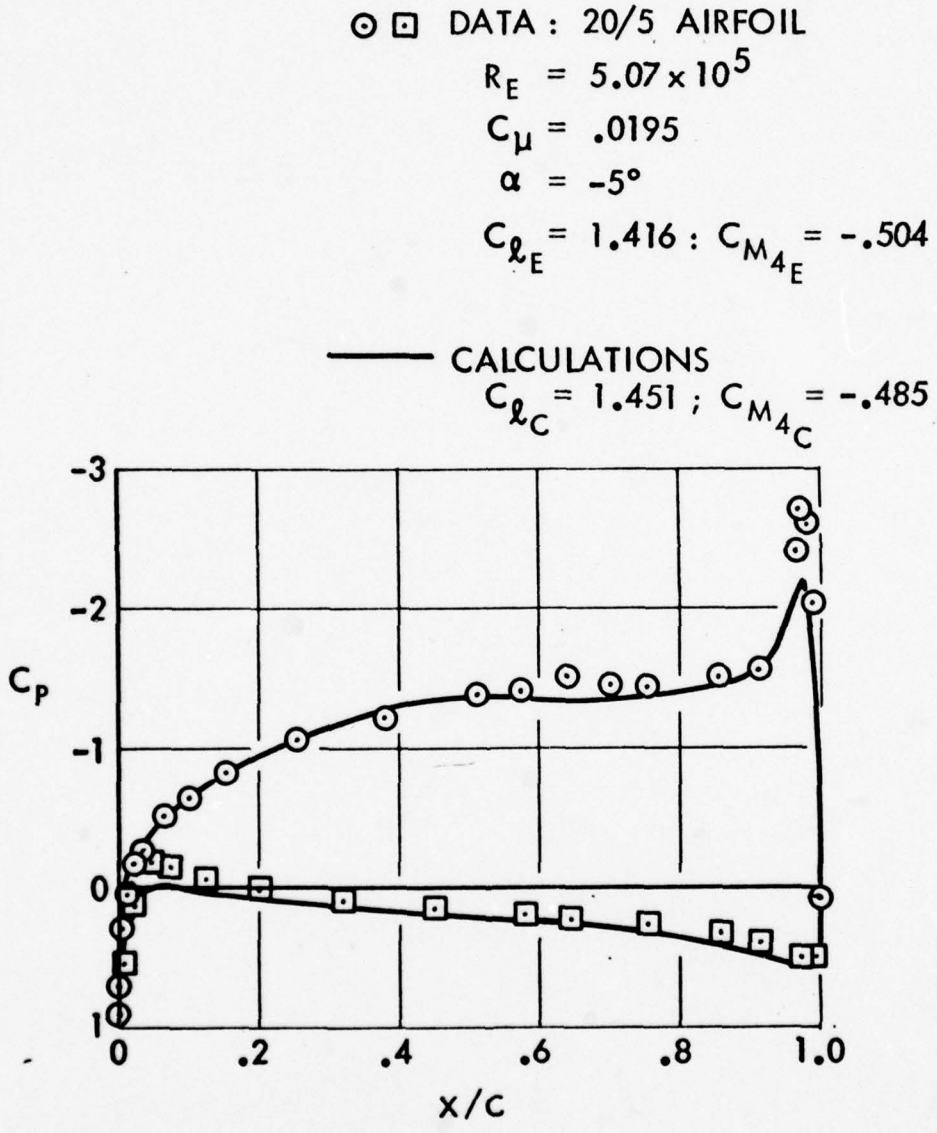

Figure 10. Comparison Between Calculated and Measured Pressure Distributions for a 20% Cambered Ellipse, $C_\mu = .02$.

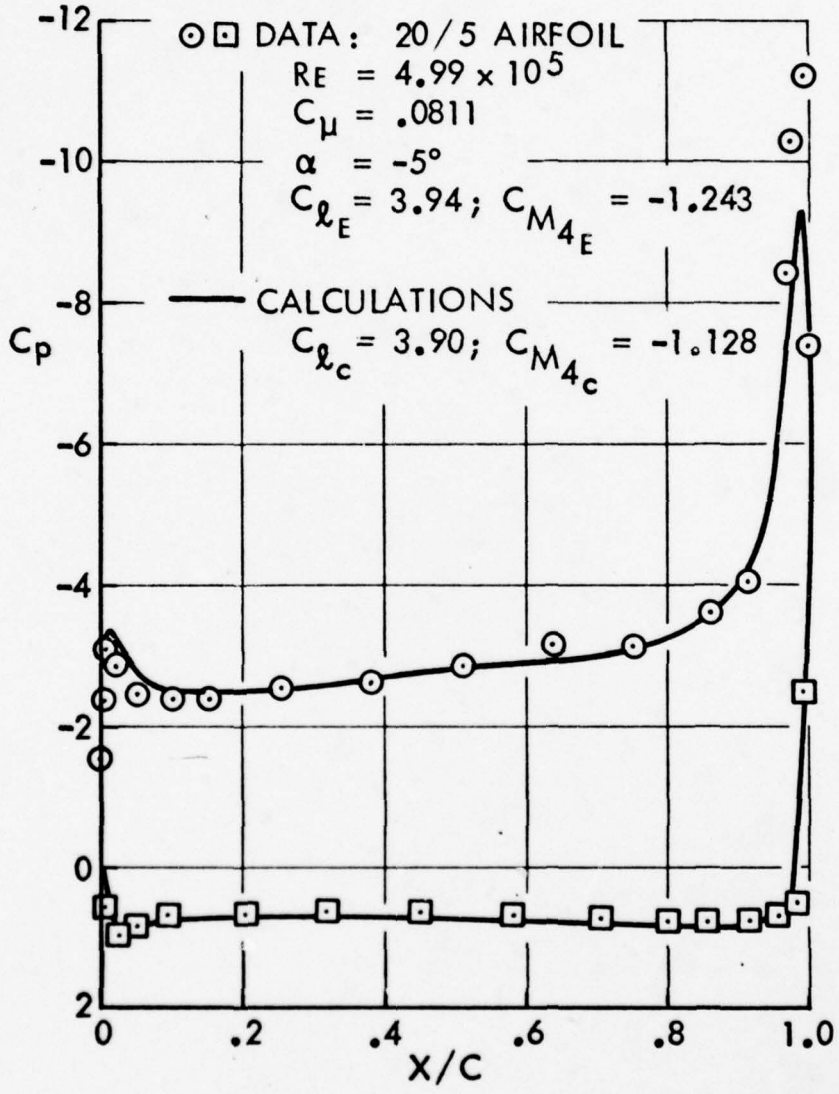

Figure 11. Comparison Between Calculated and Measured Pressure Distributions for a 20% Cambered Ellipse, C_μ = .0811.

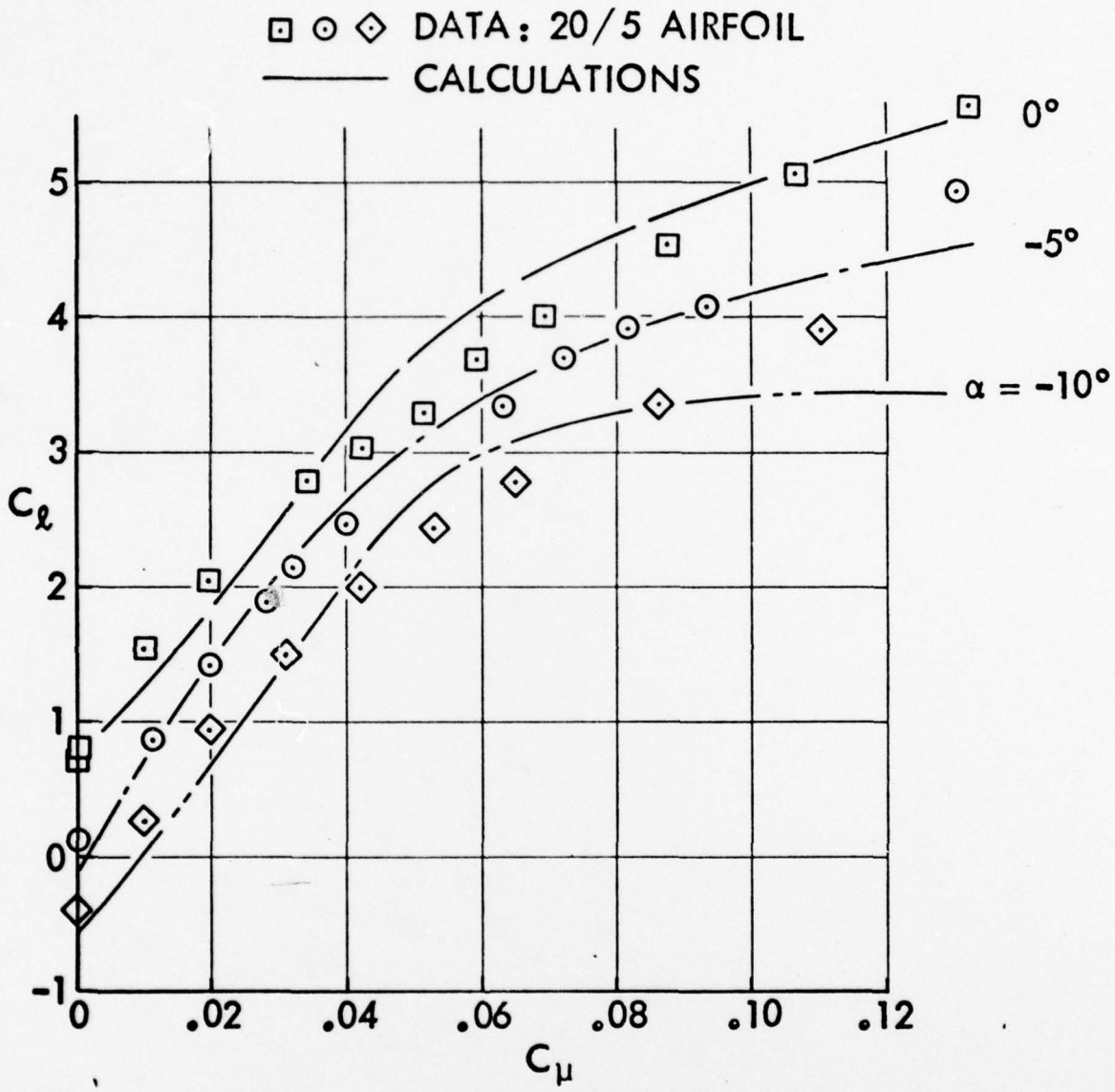

Figure 12. Comparison Between Calculated and Measured Lift Coefficients for a Range of Momentum Coefficients.

inverse logarithmic spiral model, however, as shown on Figure 14, is not good and, in fact, the theoretical analysis predicts much greater lift capability than was found experimentally. A comparison of Figures 13 and 14 show that while the analysis suggests an improved $C_\ell - C_\mu$ curve for Model 100A beyond a $C_\mu > 0.02$, comparison of the experimental results indicates no improvement in performance of Model 100A over Model 100. No explanation is currently available to account for the lack of agreement between theory and experiment for the non-circular trailing-edge model. It does, however, indicate the need for further correlational work for non-circular trailing-edge airfoils.

Figure 15 is shown to indicate that a difficulty still exists in the prediction of drag forces. That the drag predicted by the Squire and Young drag formula is in better agreement with experiment than that predicted by the integration method is surprising since separation effects are not included in the Squire and Young method. Other correlations not shown here display the same trend as shown on Figure 15 for the pressure and skin friction integration procedure. At first this lack of correlation was blamed on the experimental data, since the program was correlating well with overall pressures, particularly the base pressure as well as with overall circulation levels. After some thought it was realized however that good correlation on overall pressure distributions by no means guarantees good drag predictions. For example, a difference between calculated and experimental lift coefficient, say of 0.05 at a moderate blowing coefficient, would be considered insignificant, while the same increment for drag would be totally unacceptable. It appears that the entire drag preidction methodology should be evaluated in much more detail in order that a satisfactory procedure may be developed. For drag purposes, pressures should be displayed against a much more sensitive surface parameter than x/c. Similarly, the integration procedure whould be thoroughly investigated to determine its role in the drag prediction process.

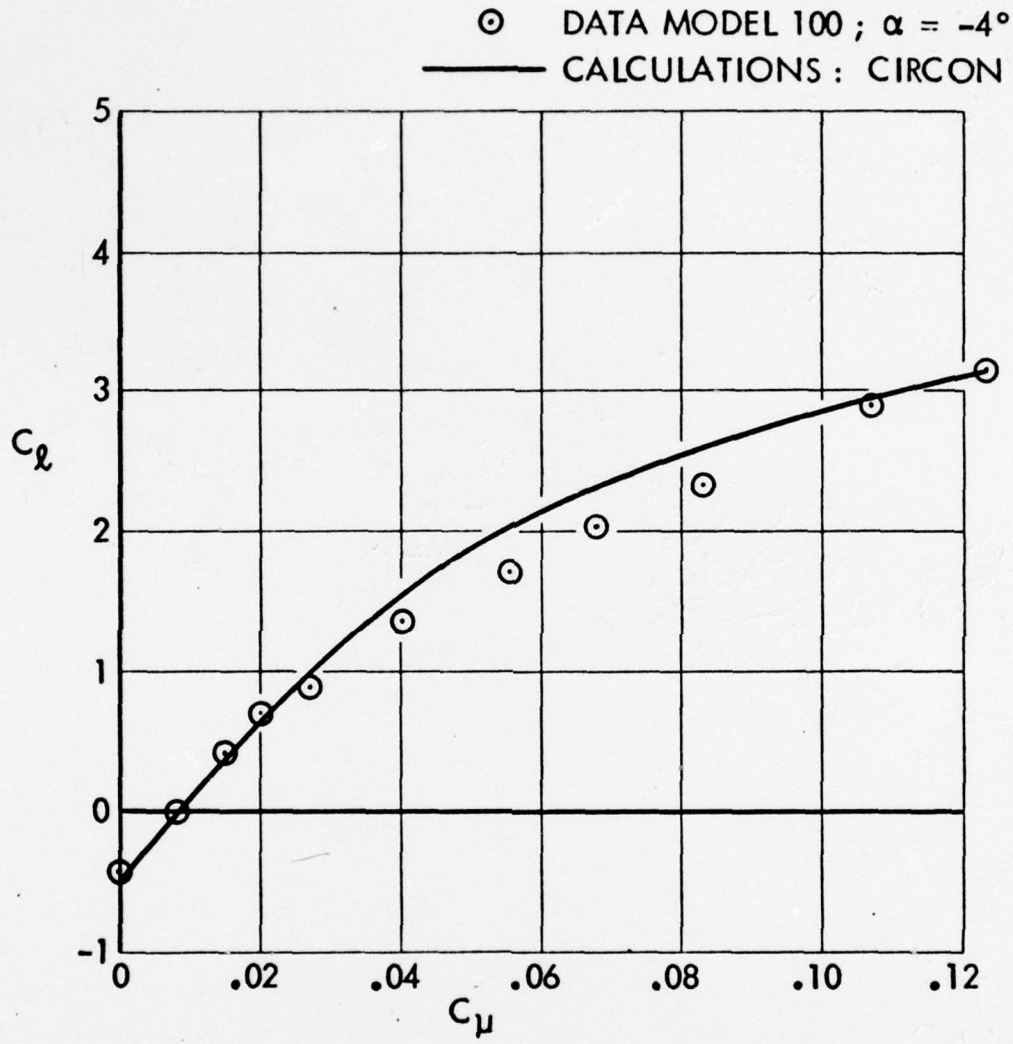

Figure 13. Comparison Between Calculated and Measured Lift Coefficients for a Range of Momentum Coefficients.

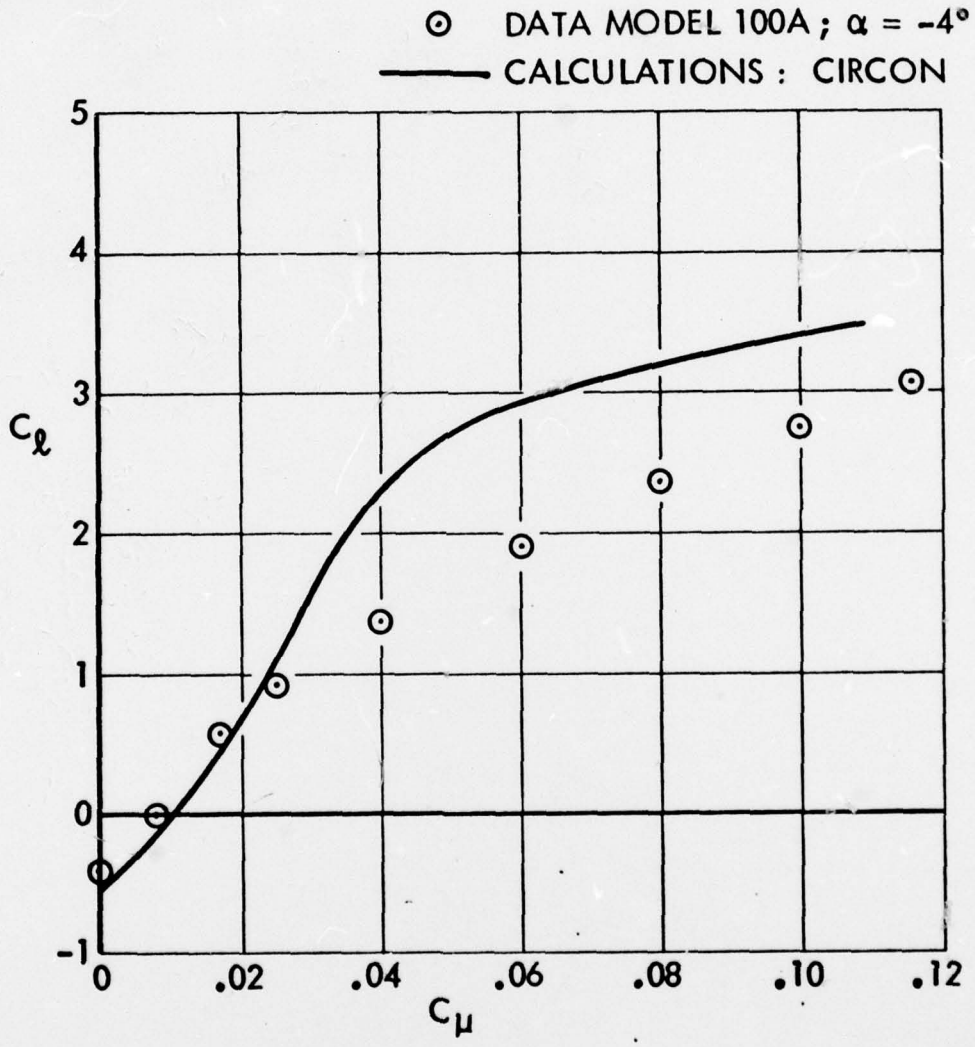

Figure 14. Comparison Between Calculated and Measured Lift Coefficients for a Range of Momentum Coefficients.

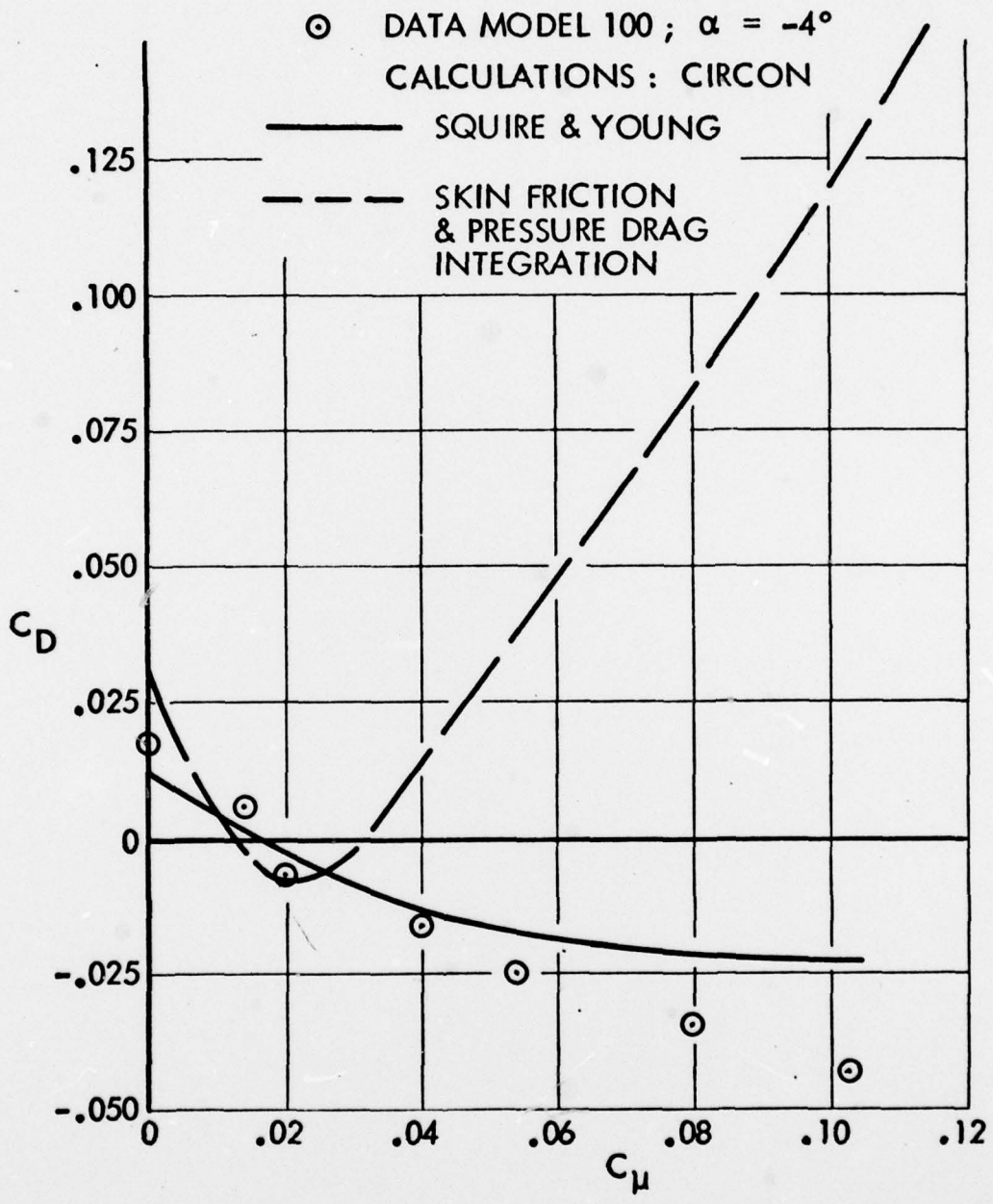

Figure 15. Comparison Between Calculated and Measured Drag Coefficients for a Range of Momentum Coefficients.

CONCLUSIONS

The initial results of comparisons with experiment are very encouraging. The method was successfully applied over a wide range of momentum coefficients including the zero blowing case. A current lack of measured shear stress distributions has precluded the correlation between theory and experiment, and the question remains, is the shear stress closure model the best possible one, or should improved or alternative models be considered. Airfoils with trailing-edges other than circular need to be investigated in considerably more detail than has currently been accomplished. Much more drag correlation work must also be carried out before a particular drag prediction procedure can be recommended.

REFERENCES

1. Dvorak, F.A., "A Viscous/Potential Flow Interaction Analysis for Circulation-Controlled Airfoils", Prepared for Contract N62269-74-C-0316, Naval Air Development Center, Warminster, Pennsylvania, December 1975.

2. Kind, R.J. and Maull, D.J., "An Experimental Investigation of a Low-Speed Circulation-Controlled Aerofoil", The Aero. Quart., Vol. XIX, May 1968, pp. 170-182.

3. Thwaites, B. (ed.), Incompressible Aerodynamics, Oxford University Press, 1960, pp. 198-200.

4. Dvorak, F.A. and Woodward, F.A., "A Viscous/Potential Flow Interaction Method for Multi-Element Infinite Swept Wings", NASA CR-2476, November 1974.

5. Schlichting, H., Boundary Layer Theory, 4th ed., McGraw Hill, N.Y., 1960, pp. 147-151.

6. Curle, H., "A Two-Parameter Method for Calculating the Two-Dimensional Incompressible Laminar Boundary Layer", J.R. Aero. Soc., Vol. 71, 1967.

7. Granville, P.S., "The Calculation of Viscous Drag of Bodies of Revolution", David Taylor Model Basin Report 849, 1953.

8. Schlichting, H. and Ulrich, A., "Zur Berechnung Des Unsellages Laminar-Turbulenten" (On the Calculation of Laminar-Turbulent Transition), Jahrbuch 1942 Der Deutschen Luftfahrt-Forschung.

9. Coles, D.E., "Measurements in the Boundary Layer on a Smooth Flat Plate in Supersonic Flow", Jet Propulsion Lab. Report No. 20-69, 1953.

10. Gaster, M., "The Structure and Behavior of Laminar Separation Bubbles", ARC 28-226, 1967.

11. Nash, J.F. and Hicks, J.G., "An Integral Method Including the Effect of Upstream History on the Turbulent Shear Stress", Proceedings Computation of Turbulent Boundary Layers -- 1968, AFOSR-IFP-Stanford Conference, Vol. 1, Stanford University, Dept. Mech. Eng., Stanford, California.

12. Kline, S.J., Morkovin, M.V., Sovran, G. and Cockrell, D.J. (ed.), Proceedings of Computation of Turbulent Boundary Layers, 1968 AFOSR-IFP-Stanford Conference.

13. Dvorak, F.A., "Calculation of Turbulent Boundary Layers and Wall Jets over Curved Surface", AIAA J., Vol. 11, No. 4, April 1973, pp. 517-524.

14. Kind, R.J., "Calculation of the Normal Stress Distribution in a Curved Wall Jet", The Aero. J., Vol. 75, May 1971, pp. 343-348.

15. Prandtl, L., Ludwig Prandtl Gesammelte Abhandlungen, (W. Tollmien, H. Schlichting and H. Goertler, eds.) Springer 1961, p. 775.

16. Sawyer, R.A., "Two-Dimensional Turbulent Jets with Adjacent Boundaries", Ph.D. Thesis, Cambridge Univ., 1942.

17. Wilson, D.J. and Goldstein, R.J., "Turbulent Wall Jets with Cylindrical Streamwise Surface Curvature", J. Fluids Eng., Vol. 98, Series 1, No. 3, September 1976, pp. 550-557.

18. Jones, D.G., "The Performance of Circulation-Controlled Aerofoils", *Ph.D. Dissertation, Cambridge Univ.*, 1970.

19. Seebohm, T. and Newman, B.G., "A Numerical Method for Calculating Viscous Flow Round Multi-Section Aerofoils", The Aero. Quart., Vol. 26, August 1975, pp. 176-188.

20. Squire, H.B. and Young, A.D., "The Calculation of the Profile Drag of Airfoils", Brit. Aero. Res. Coun. R and M 1838, 1937.

21. Abramson, J., "Two-Dimensional Subsonic Wind Tunnel Evaluation of a 29% Thick Circulation-Control Airfoil", ASED Tech. Memo 16-76-42, December 1975.

22. Williams, R.M. and Howe, H.J., "Two-Dimensional Subsonic Wind Tunnel Tests on a 20% Thick, 5 % Cambered Circulation-Control Airfoil", Tech. Note AL-176, NSRDC, Washington, D.C., August 1970.

23. Kizilos, A.P., "Experimental Determination of Separation for an Underexpanded Coanda Jet", Honeywell Memo. 10232, February 1968.

APPENDIX "A"

COANDA JET DETACHMENT

Introduction

A circulation-controlled airfoil operating in a high subsonic Mach Number free stream may or may not experience the phenomenon of Coanda jet detachment. The Coanda jet nozzles are convergent by design so that when they operate choked, the jet flow downstream of the nozzle exit plane can reach very high fully expanded Mach Numbers of the order of 1.8 or more. At these Mach Numbers, shock-induced separation of the Coanda jet is possible. Experiments demonstrating such a phenomenon have been conducted by Honeywell (Ref. 23) for jets expanding over a circular cylinder in a quiescent stream.

A brief study was undertaken to see if the phenomenon of jet detachment could be studied using a method of characteristics program available through Boeing Computer Services. Unfortunately, the program is completely inviscid in nature, and while viscous effects may be dominant, they have not been considered.

The nozzle pressure ratios of interest in this study are greater than three, assuring an initially supersonic plume. The origin of the plume is a choked convergent nozzle. The configuration is generally illustrated in Figure A1. Note that since the analysis is inviscid, there are two key parameters; (1) the nozzle pressure ratio, P_{TN}/P_{∞}, and (2) the nozzle exit height to Coanda surface radius, b/a. All studies to date consider a plume exhausting into a quiescent atmosphere. For this problem, a constant pressure boundary, at ambient pressure, may be specified as the boundary between the supersonic plume and the quiescent ambient in the MOCHA Program. The solution of a subsonic ambient flow would require some coupling with an external flow solution

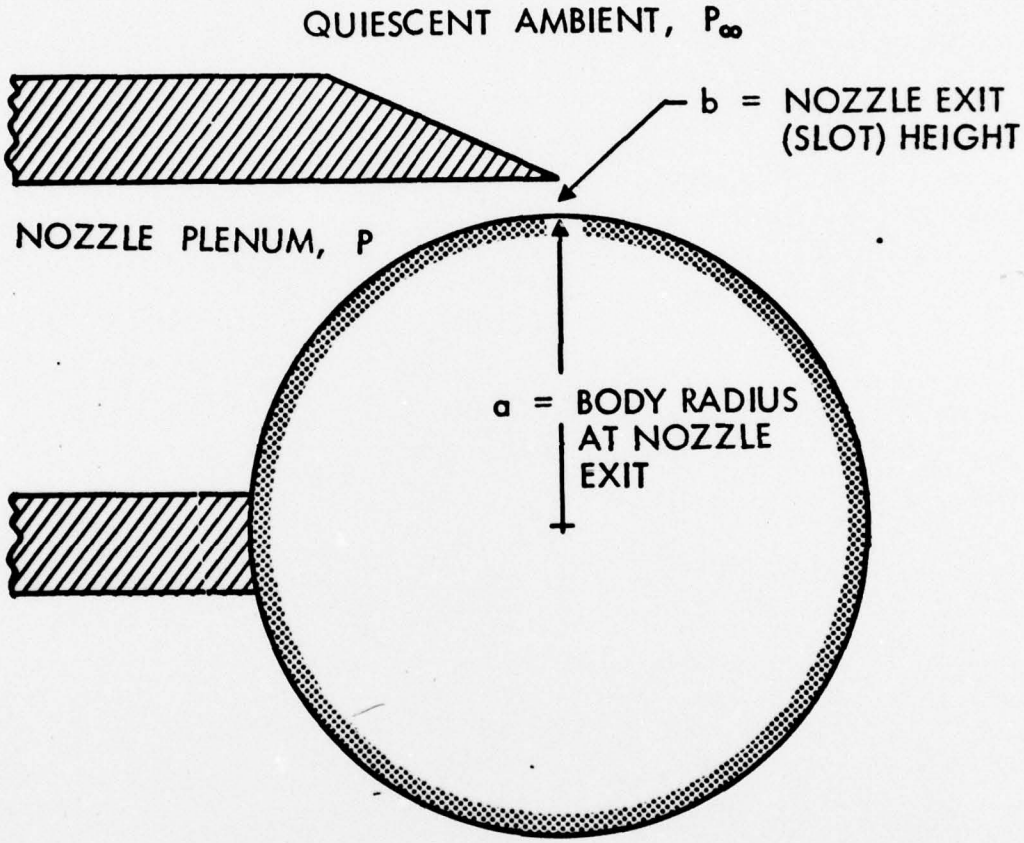

Figure A1. Schematic of Honeywell Test Apparatus for Coanda Blowing Jet Tests.

to determine plume-edge pressure. That was not considered at this time. Edge mixing effects, which may be very important in the real flowfield, are neglected, as are all viscous effects including surface boundary layer development. The purpose of the study is to investigate the effects of Coanda expansion surface shape on the pressure distribution on that surface. The hope is that the inviscid solution will at least demonstrate the trends of surface shape effects.

Results

A moderate pressure ratio case from the Honeywell data was selected for comparison with the MOCHA Program. This case has a nozzle pressure ratio of about 3.61 and b/a = 0.16. The surface pressures, both calculated and experimental, are shown in Figure A2. The agreement between analysis and data is not particularly good. Experimentally, subsonic flow was detected in the plume after turning about 75 degrees around the cylindrical surface from the exit.

The pressure ratio for this case is in the region of interest for circulation-controlled airfoils. In an attempt to investigate the effects of surface curvature on the plume development, a simple 2:1 ellipse oriented with the major axis along the exit flow direction was chosen as the next step. The results are shown in Figure A2, together with the baseline circular cylinder (P_{TN}/P_{∞} = 3.61, b/a = 0.16 for both cases). The compressing of the pressure curve in Figure A2 for the ellipse case is in part due to the fact that it is plotted against surface angle, and the ellipse has less turning for a given length initially than a circle with the same exit radius. Although had the comparisons been plotted against surface distance, the conclusions would remain the same.

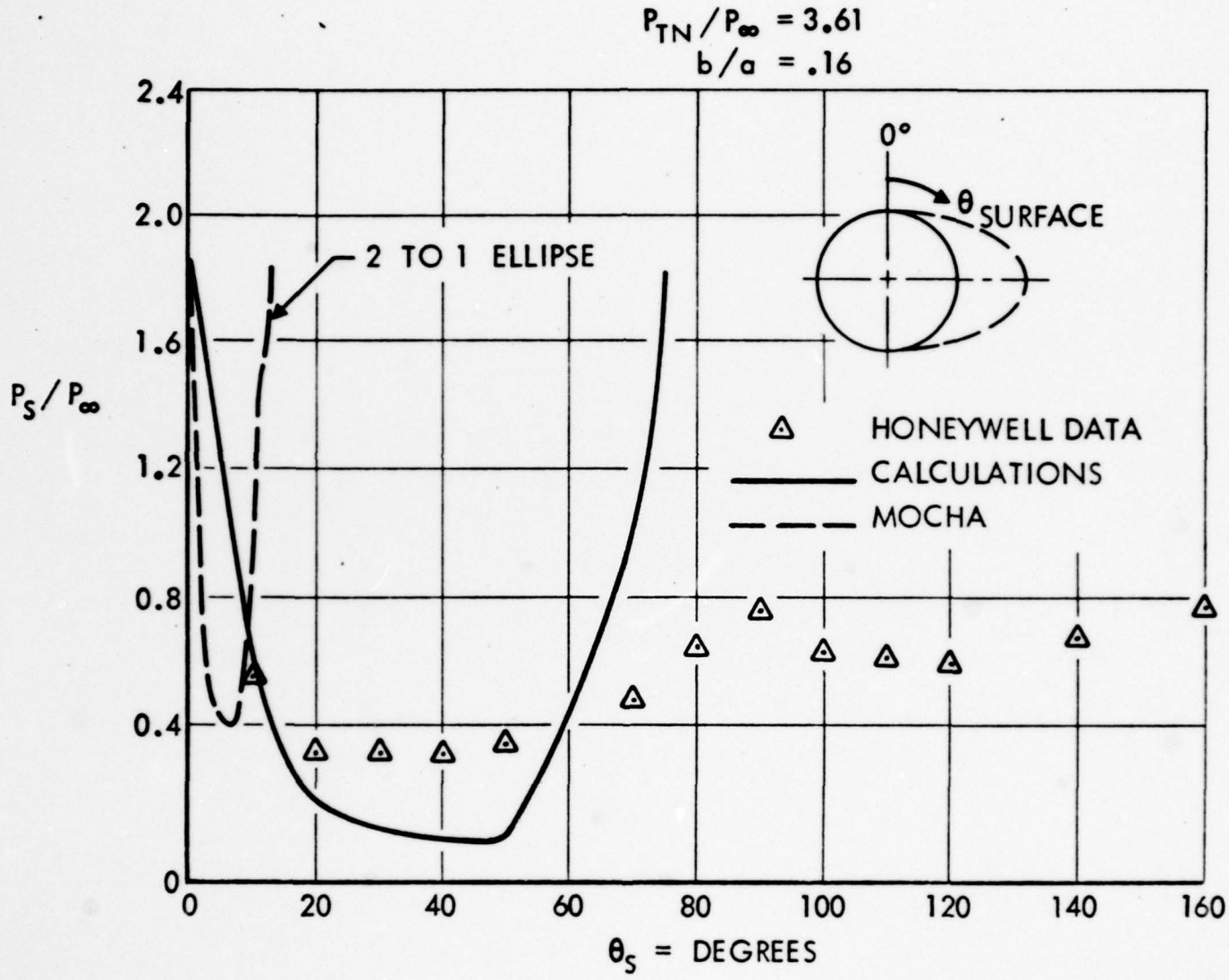

Figure A2. Comparison Between Calculated and Measured Surface Pressures.

More important, however, is that with less surface turning (ellipse), the surface and plume edge are in closer proximity (and there is less overexpansion on the surface) so that the expansion reflected from the surface interacts with the constant pressure plume edge sooner, producing a reflected compression which interacts with the surface sooner than if the surface had been turned further (circular cylinder).

Discussion

The primary problem area for these underexpanded plumes with constant pressure boundaries is that the outer edge expansion is independent of body shape. The body shape affects the plume edge shape downstream of the initial expansion. The plume edge expansion reflects from the body surface, then interacts with the constant pressure boundary, and is reflected as a compression. This is (neglecting mixing effects which may be very important) the primary expansion-compression system in the plume.

Considering the case of a convergent nozzle, the control that may be exerted using Coanda expansion surface shape as the variable is simply to turn the surface away from the compression more rapidly. This delays the impingement of the compression on the surface and produces surface expansion to counter the compression effect.

The role of viscosity in modifying the flow pattern is a complicated one, but from the results of Figure A2, essential to any analysis if an accurate representation of the flow field is to be expected. If a mixing layer model could be employed, it would result in less initial expansion of the flow, and consequently, not as strong a subsequent compression--more in line with the observed data. In the circulation-control airfoil

application, the absence of viscous effects in the analysis would probably lead to a grossly innaccurate representation of the flow field.

Because viscous effects have been excluded in the analysis, no further comparisons were made using the MOCHA Program. Indications are, however, that increased surface curvature away from the nozzle exit plane (with the surface acting like one-half of a divergent nozzle) increases the ability of the jet plume to stay attached.

Recommendations

A thorough analysis of circulation-controlled airfoils at high subsonic Mach numbers much include viscous effects. It is believed that this can be accomplished by replacing the inviscid calculation in Program CIRCON by a transonic method (Garabedian and Korn, or Jameson) capable of predicting shock waves anywhere on the airfoil surface, and particularly on the Coanda surface in the trailing-edge region of the airfoil. In addition, compressibility effects must be included in the finite-difference wall jet calculation if accurate predictions of separation are to be expected.